SAYAM Vol-I, Issue-II (December, 2023), Page No-34-50

Journal Homepage: https://sayamjournal.com/

Article

Identification of Small Molecule-Based Inhibitor of Estrogen Receptor: A Computational Approach

Zaina Waris[a,b], Payal Datta[a,c], Samima Khatun[a,b], Prabuddha Bhattacharya[a*]

[a]Department of Chemistry, Mrinalini Datta Mahavidyapith, Kolkata-700051
[b]Department of Biochemistry, West Bengal State University, Kolkata-700126
[a]Department of Chemistry, Christ - Deemed to be University, Bengaluru-560029
[*]Corresponding author: b.prabuddha3@gmail.com

ARTICLE INFO

Keywords:
Breast cancer, Estrogen receptor alpha, Molecular docking, Binding affinity, MD simulation, ADMET properties, and DFT studies.

Received: 03/08/2023
Accepted: 20/12.2023
Date of Publication: 30.12.2023

ABSTRACT

Breast cancer is the prevailing type of cancer impacting women worldwide. Estrogen receptor (positive) breast tumors constitute approximately 75% of the total breast cancer cases. Virtual screening of 200 small organic molecule-based ligands against estrogen receptor alpha (ERα) was performed using AutoDock Vina. The molecules were ranked according to their binding affinity values, and their interactions with the residues of the active site were thoroughly examined. Computational prediction of the ADMET properties was also performed to understand the pharmacokinetic (PK) properties of the screened molecules. L10 exhibited the highest binding affinity. (-12.311 kcal/mol), which was higher than the FDA-approved drug Afimoxifene (-10.46 kcal/mol). DFT studies with L10 revealed favorable structural and electronic properties augmenting the drug-like nature of the molecule. The apo-protein and the protein-ligand complex corresponding to L10 were subsequently subjected to 100ns all-atom MD simulation using GROMACS with CHARMM 36 force field. Analysis of the simulation trajectory indicated reasonably high stability of the corresponding protein-ligand complex. Thus, our current study shows that L10 can be a potentially strong inhibitor of the estrogen receptor alpha (ERα), and hence it may be studied further for developing drugs against breast cancer.

Introduction

The uncontrolled proliferation of cells beneath one or both breasts is the underlying cause of breast cancer. Those cells might proliferate to adjacent cells and thus become metastatic (https://webmd.com). Breast cancer is globally recognized as the most common and intricate disease, representing the secondary factor contributing to women's cancer-related death (Chen et al, 2023). A prevalent subtype of breast cancer is categorized as estrogen receptor (ER)-dependent breast cancer. About 80% of breast tumors are ER-positive. Out of this total of 80%, approximately 60% of instances occur in women before menopause, while 75% are seen after menopause.

The tumors rely on estrogens for growth and survival due to the overexpression of estrogen receptors (ERs) within them. Endocrine medications that disrupt the estrogen-ER signaling pathway can be used to target hormone receptor-positive tumors. Tamoxifen is a part of the class of medications known as selective oestrogen receptor modulators, or SERMs. These drugs are frequently used to treat oestrogen receptor-positive breast cancer. SERMs inhibit the growth-promoting effects of estrogen because they bind to the ER and prevent estrogen from binding. Another class of medication used in Women in the postmenopausal stage diagnosed with ER-positive breast cancer is known as aromatase inhibitors (AIs), through preventing the conversion of androgens into oestrogens by the enzyme aromatase, AIs lower estrogen production (https://webmd.com; Chen, 2011). Targeting hormone-sensitive pathways, these therapies significantly reduce recurrence risk, improving survival rates. The prognosis for breast tumors that are ER-positive is typically favorable due to the success of endocrine therapies in disrupting hormone-driven pathways (Davies et al, 2011; Nicholson & Johnston, 2005). The development of resistance to hormonal therapy in breast cancer patients having estrogen receptor-positive tumors poses an intricate challenge, involving mechanisms like disrupted estrogen receptor signaling pathways, activation of alternative pathways, and epigenetic changes. Strategies to overcome resistance include combination therapies, next-generation endocrine treatments, precision medicine approaches, and immunotherapy. The FDA has authorized multiple medications for the management of breast cancer that are positive for estrogen receptors. Notable examples include Anastrozole, Letrozole, Elacestrant, Exemestane, Tamoxifen, Fulvestrant, Palbociclib, Ribociclib, and Abemaciclib (Osborne & Schiff, 2011; 7. Hanker, 2020; US F DA).

Targetable biomolecules are specific proteins or genes that are overexpressed or have undergone mutations in some breast cancer subtypes. These biomolecules have emerged as potential targets for precision medicine strategies, (**Figure 1**) enabling more individualized and efficient therapies. Let us briefly discuss some important druggable targets for breast cancer.

The progression of breast cancer is driven by a complex landscape of molecular changes. There is an increase in the amount of the protein known as human epidermal growth factor receptor 2 (HER2), which controls cell division and development. This upregulation of HER2 expression is associated with the development and advancement of specific cancer types, constituting 20-25% of breast cancers (Hsu & Hung, 2016). The signaling pathway known as PI3K/AKT/mTOR plays a crucial role, in orchestrating diverse biological functions which include metabolism, growth, and survival. Dysregulation of this pathway, notably mTORC1 and mTORC2 complexes, contributes to uncontrolled growth (Miricescu et al, 2021). Hormone receptor-positive breast cancer, characterized by estrogen and progesterone receptor expression, thrives on hormone-driven survival signals facilitated by local estrogen production via aromatase activity (Edris et al, 2023). Cyclin-dependent kinases CDK4 and CDK6 mediate the cell cycle progression in a complex manner, their activation culminating in the phosphorylation of retinoblastoma protein and subsequent E2F-driven cell cycle gene expression. Understanding these molecular intricacies underpins targeted therapeutic approaches for breast cancer (Lee, 2023). A protein essential for inhibiting tumor growth is produced by the BRCA1 gene, which is inherited from both parents. Breast and ovarian cancer risk is increased by mutations in this gene. Cancer risk is also increased by BRCA2 mutations. These mutations are found through genetic testing (https://www.cancer.gov).

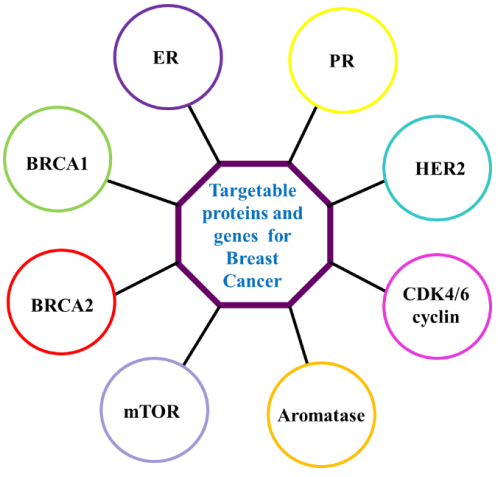

Figure 1 Representation of biomolecules that can be targeted for breast cancer treatment.

The estrogen class of steroid hormone interacts with the ER, a crucial receptor in the body, serving as its natural substrate. The predominant perspective regarding the role of estrogen in breast cancer posits that it functions as a facilitator for cancer progression by promoting the growth and division of breast tissue, thereby posing a potential risk for cancer-promoting mutations. The prevailing view on estrogen's role in breast cancer suggests that prolonged estrogen exposure heightens the risk of mutations by fostering DNA replication errors. This occurs as estrogen propels cell cycle progression, particularly from the G1 to the S phase, amplifying opportunities for mutation occurrence. Estrogen metabolism, converting estradiol to metabolites like catechol estrogens, generates reactive intermediates capable of inducing DNA damage. Unrepaired DNA damage, coupled with estrogen-induced oxidative stress and subsequent genomic instability, contributes to cancer initiation. Hence, estrogen serves as a facilitator for breast cancer progression, promoting cell division and proliferation while posing a potential threat of cancer-promoting mutations (Yager & Davidson, 2006).

4-Hydroxytamoxifen, also known as Afimoxifene, is the active metabolite of tamoxifen, a selective modulator of the estrogen receptor (ER) that exhibits estrogenic antagonism in breast cancer, showcasing a heightened affinity for ERα compared to tamoxifen that is frequently used in the chemopreventive and therapeutic treatment of breast cancer (Rocha-Roa, 2023).

ERα belongs to the superfamily of transcription regulators known as nuclear hormone receptors. The human estrogen receptor (ERa) exhibits a conventional structure that is conserved among all steroid receptor family members. The complete length of ERα consists of 595 amino acid residues and has a molecular weight of 67 kDa. It comprises six identified functional areas A–F (**Figure 2**). The A/B domain at the amino-terminal portion of all steroid receptors has the most variable region; this region is in control of the hormone-independent activation function known as AF-1. The DNA-interacting domain resides within the C domain, termed the DBD. The hinge region of the D domain is thought to be involved in the binding of co-regulatory proteins. The carboxy-terminal E and F domains contain the ligand-binding domain (LBD) (**Figure 3**). This particular region not only modulates the agonist effects of non-steroidal antiestrogens but also harbors supplementary binding sites that facilitate the interaction with co-regulator molecules. (https://www.cancer.gov).

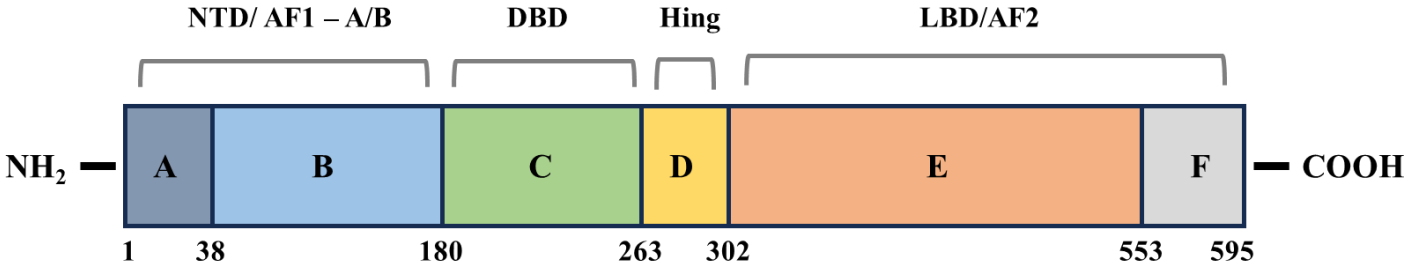

NTD= N-terminal Transactivation Domain
AFs= Independent activation functions
LBD= DNA Binding Domain
Hing= Determines the functional synergy between AF-1 and AF-2 in the quantitative response to estradiol and tamoxifen.

Figure 2 a) Diagram representing the structural and functional domains of the ER.

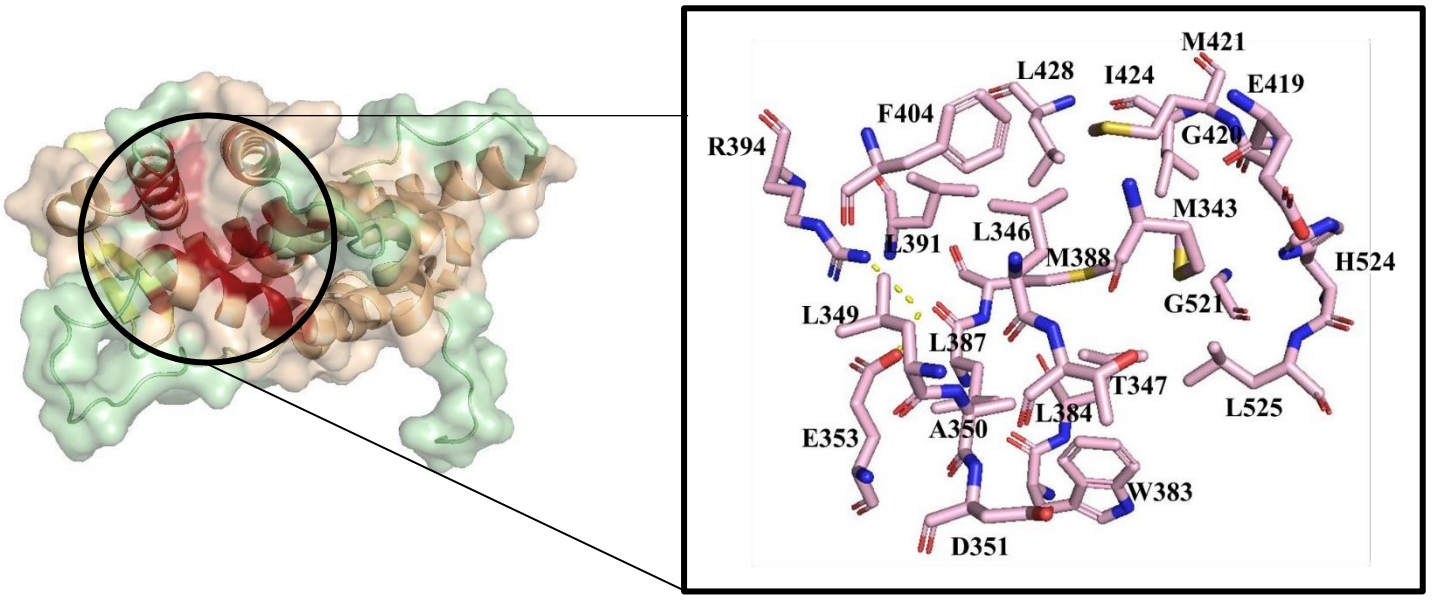

Figure 3 Active site Residues of ERa

In this work, we carried out virtual screening and ADMET profiling of two hundred small organic molecules against ERα to identify the potential inhibitors with reasonably good drug-likeness. To comprehend the dynamic behavior of the ligand in the binding pocket, a subsequent MD simulation of the top-ranked candidate was carried out. DFT studies were done to correlate the molecule's structural and electrical characteristics connect to its potential for therapeutic use and biocompatibility.

1. Materials and Methods

1.1. Molecular Docking and Pharmaco-Kinetic Predictions

The RCSB PDB was the source of the ERa-protein (PDB ID: 3ERT) (https://www.rcsb.org/search). Hetero atoms (water and co-crystallized ligand) were removed using UCSF Chimera (Pettersen et al, 2004). The incorporation of polar hydrogen and assignment of gasteiger charges [Gasteiger & Marsili, 1978). were done using Auto Dock Tools (ADT) (Morris et al, 2009). To generate the ligand library usedfor virtual screening (https://pubchem.ncbi.nlm.nih.gov/) similarity-search was done using the structures of estradiol and tamoxifen (FDA-approved drugs). Furthermore, some of the candidates were also obtained through pharmacophoremodeling on ZINCpharmer (http://zincpharmer.csb.pitt.edu/) using reported molecules showing strong inhibitory action against ER (Saha et al, 2019). 3D structures for the rest of the ligands were made using ChemDraw 3D. Subsequent geometry optimization and protonation considering the physiological pH were done using MMFF94 implemented through Avogadro. ADT was used for generating the required pdbqt files. A three-dimensional grid is generated around the estrogen receptor protein. The grid box with dimensions of 30Å, 16Å, and 20Å (along the X, Y, and Z directions, respectively) with a spacing of 1Å was set using Chimera. Its centre was at X= 28.70, Y= -0.80, and Z= 27.16. Search exhaustiveness was kept at 32. The AutoDock Vina was employed to execute the docking simulation. (v1.2.3) (Eberhardt et al, 2021). The co-crystallized ligand (4-hydroxytamoxifen) was separately re-docked into the protein (PDB ID: 3ERT) using AutoDock Vina with the same docking parameters (grid center, grid dimensions, exhaustiveness). The docked poses were visualized using PyMOL and Discovery Studio (2021 client version). ADMET properties of all the 200 candidates were computationally predicted using SwissADME (Daina et al, 2017) and pkCSM server (Pires et al, 2015). The results were also used to interpret the drug-likeness of the molecules through validation of Lipinski's rule (Lipinski et al, 2001).

1.2. Molecular Dynamics Simulation (MDSimulation)

Using GROMACS 2022, all-atom molecular dynamic simulations lasting 100 ns were performed on the molecule displaying the lowest binding energy and the maximum binding affinity (Bauer, 2022). The protein topology was constructed using the force field CHARMM36 (Huang, 2013). Swiss Param Server was used to build the ligand topology and data that were compatible with GROMACS (https://www.swissparam.ch) (Zoete et al, 2011). After elimination with the Na+ and Cl-ions at 0.15 (M) buffer concentration (physiologically isotonic state) (Boonstra et al, 2016], the TIP3P water model was utilised to solve the system (Mark & Nilsson, 2001). The steepest descent algorithm was then used to minimize the energy of the system, with forces lower than 10.0 kJ/mol and/or a maximum step count of one million. 1 ns NVT and 1 ns NPT, were used to equilibrate the ensemble. Using GROMACS 2022's built-in functions, the final trajectory file was examined after the periodic boundary conditions (PBC) were changed. To determine the following geometric parameters: i) radius of gyration (Rg); ii) solvent accessible surface area (SASA); iii) root mean square deviation (RMSD) for the protein Cα, ligand, and complex; and v) interaction energy (Coulomb Short range and Lennard Jones Short range).

1.3. Density Functional Theory (DFT)

The candidate with the highest binding affinity was used in DFT calculations using Gaussian 09W software (Frisch et al, 2016). The split valence basis set 6-311+G(d,p) with Becke's three-parameter hybrid functional B3LYP was employed. for the computational approach (Petersson et al, 1998; Koopmans, 1934). The geometry-optimized structure obtained from these calculations was utilized for subsequent analyses, including molecular orbital studies and the generation of electrostatic potential maps. The values of Electron Affinity (EA) and Ionisation Potential (IP) were obtained by applying Koopman's theorem (Murry et al., 1996; Boukabcha et al., 2015; Demir 2019). Other important properties, such as electronegativity, chemical potential, chemical hardness, chemical softness, and the electrophilicity index, were subsequently determined using the values obtained for Ionisation Potential (IP) and Electron Affinity (EA). For comprehensive formulas, refer to the supplementary information.

2. Results and Discussion

2.1. Docking studies

The study of molecular docking using AutoDock Vina with the ligand library comprised of 200 molecules revealed a wide variety of binding affinities and interactions. To

validate the docking protocol, the co-crystallized ligand (4- hydroxytamoxifen) was re-docked at its respective binding site for the protein. A reasonably low average RMSD of 1.934 was obtained for the best-docked pose as compared to the crystal structure (**Figure 5**). The robustness of the utilised docking parameters increases with decreasing average RMSD because they can more closely resemble the complex's initial crystallographic bound state. An RMSD value below 3Å is acceptable for the validation of the docking parameters (Debnath et al, 2021). The fact that the re-docked poseand the co-crystal form of 4-hydroxytamoxifen interacted with almost the same residues (21 common residues out of 22) in the binding pocket further substantiated our docking protocol (**Table 2**).

Amongst the 200 screened ligands, binding affinities of ligands **L10, L12, L13, L15, L33, L69, L167, and L179** were found to be greater than FDA-approved drug afimoxifene (-10.46 kcal/mol). **L10, L12, L13, L41,** and **L179** (**Figure 4**) emerged as the potentially best 5 drug candidates based on their binding affinities and interactions (**Figure 7**) with the protein (**Table 1**).

A careful inspection of the active site as well as the literature survey reveals that the active site binding pocket of the target protein is predominantly hydrophobic (Kumar et al, 2011) which is expected to be chemically more compatible with ligands having hydrophobic scaffolds. Thus, as expected, ligands with aryl rings and/or double bonds (having p-electron cloud) showed greater binding affinity which may be attributed to different types of hydrophobic interactions (p- p interaction, van der Waals interaction, etc.) which stabilizes the corresponding ligand-protein complexes (refer to Table 1 and the interaction table in the SI). Figures 6a, and 6b, show **L10** in the binding pocket (as per the best-docked complex) and distance (**Figure 6c**) while highlighting the role of hydrophobic interactions in stabilizing the complex.

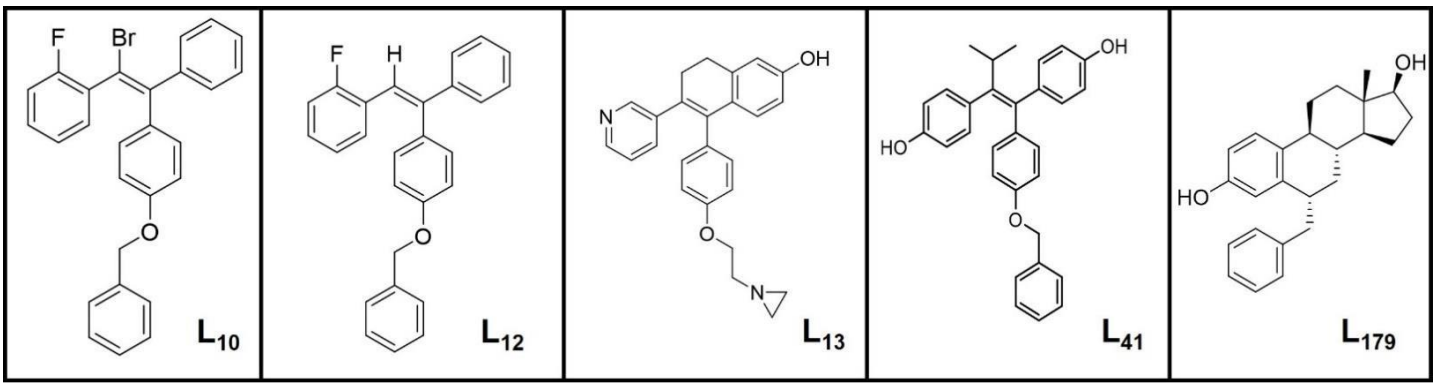

Figure 4 Structures of L10, L12, L13, L41, L17

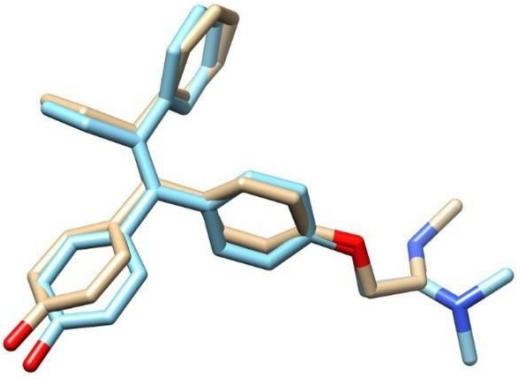

RMSD = 1.934 Å

Figure 5 RMSD (non-hydrogen atoms) of the best docked posed and the co-crystal structure of the ligand (4-hydroxytamoxifen)

The binding pocket of the active site accommodates 4-hydroxytamoxifen, with specific amino acid residues involved in the interaction. These residues include Glu353, Arg394, Met343, Leu346, Thr347, Ala350, Trp383, Leu384, Leu387, Leu525, and Asp351. Each of these residues contributes to stabilizing and positioning 4-hydroxytamoxifen within theactive site pocket, playing a crucial role in the molecular interactions between the ligand and the protein (Shiau et al, 1998).

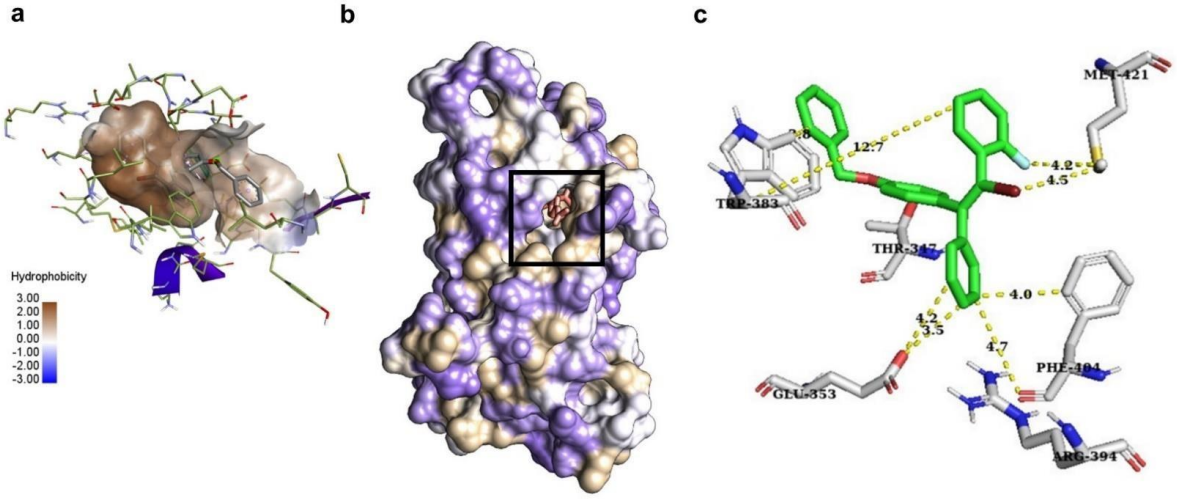

Figure 6 a) Hydrophobic Interaction of Ligand and Protein of L10, b) Hydrophobic groove of the Protein, c) Distance between L10and active site residues in Å

Table 1. Interaction of the best five docked candidates along with the reported co-crystallized ligand (4-hydroxytamoxifen) and its re-docked pose

Sl. No.	Ligands ID	Binding Affinity (kcal/mol)	Interacting Amino Acid Residues	
			Hydrogen Bonding	**Non-Covalent Interactions other than Hydrogen-Bonding**
1	L10	-12.311	-	**M343**,**L346**,**T347**,L349,**A350**,**E353**,**W383**,**L384**, **L387**,M388,L391,**R394**,F404,G420,M421,I424,L428, G521,H524,**L525**,M528
2	L12	-11.366	-	**M343**,**L346**,**T347**,L349,**A350**,**E353**,**W383**,**L384**, **L387**,M388,L391,**R394** F404,E419,G420,M421,I424, G521,H524,**L525**,M528
3	L13	-10.875	-	**M343**,**L346**,**T347**,L349,**A350**,**E353**,**W383**,**L384**, **L387**,M388,L391,**R394**,F404,E419,G420,M421,I424, L428,G521,H524,**L525**
4	L41	-12.176	-	**M343**,**L346**,**T347**,L349,**A350**,**E353**,**W383**,**L384**, **L387**,M388,L391,**R394** F404,E419,G420,M421,I424, L428,G521,H524,**L525**
5	L179	-11.08	G521,H524	**M343**,**L346**,**T347**,L349,**A350**,**D351**,**E353**,**W383**, **L384**,**L387**,M388,L391,**R394**,F404,G420,M421,I424, **L525**,M528
6	4-Hydroxytamoxifen (re-docked pose)	-10.46	**E353**,**R394**	**M343**,**L346**,**T347**,L349,**A350**,**W383**,**L384**,**L387**, M388,L391,F404,E419,G420,M421,I424,L428, G521,H524,**L525**,M528
7	OHT 4-Hydroxytamoxifen (as co-crystal)	-	**E353**,**R394**	**M343**,**L346**,**T347**,L349,**A350**,**D351**,**W383**,**L384**, **L387**,M388,L391,F404,E419,G420,M421,I424,L428, G521,H524,**L525**

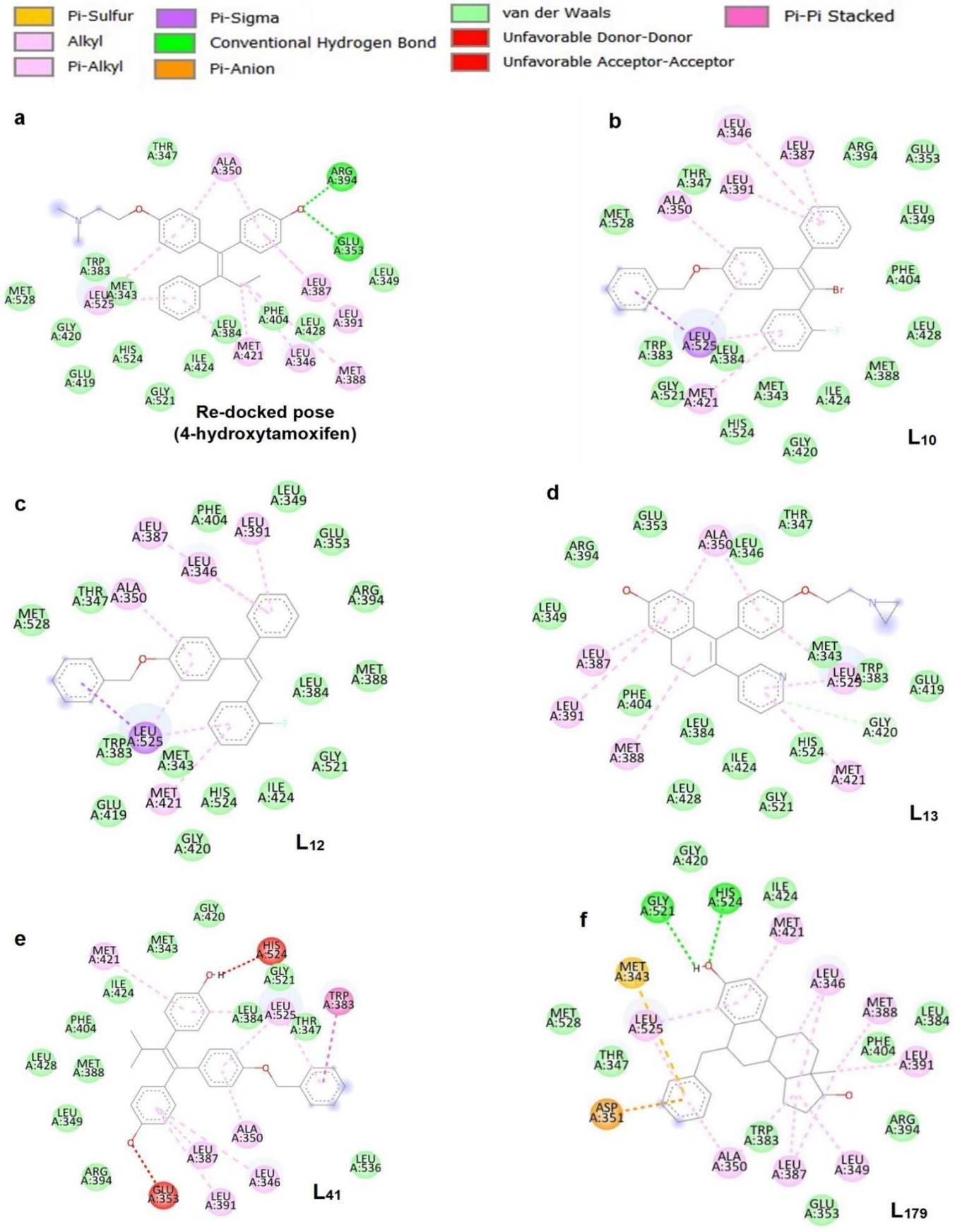

Figure 7 2D and 3D interaction of Ligand with Protein, a) co-crystalized ligand (PDB ID: OHT) b) L10, c) L12, d) L13, e) L41, f)L179

In the docking analysis, the co-crystallized ligand 4-hydroxytamoxifen interacted with 22 amino acid residues, which includes active site residues (Glu353, Arg394, Met343, Leu346, Thr347, Ala350, Trp383, Leu384, Leu387, Leu-525, and Asp-351) while the top best-docked ligands (**L10, L12, L13, L41, L179**) exhibited interactions with 21 residues each. 20 out of these 21 interacting residues for **L10, L12, L13, L41** and **L179** while 19 out of 21 matched with those of 4- hydroxytamoxifen, (**Table 2**) demonstrating a high degree of similarity in binding profiles (**Figure 7**). This underscores the reliability of the docking simulations and suggests the potential efficacy of the top best-docked ligands comparable to the co-crystallized ligand 4-hydroxytamoxifen.

Table 2. Comparison in the number of interacting amino acids

Ligand	4-Hydroxytamoxifen	L10	L12	L13	L41	L179
No. of interacting amino acids	22	21	21	21	21	21
Interacting residues in common with the reference ligand (4-hydroxytamoxifen)	-	20	20	20	20	19

1.1. ADMET studies

ADMET (Absorption, Distribution, Metabolism, Excretion, and Toxicity) properties assessment is critical in drug discovery, as it evaluates how a potential drug is absorbed, distributed, metabolized, and eliminated in the body, while also identifying potential toxicity risks. This helps in selecting compounds with favorable pharmacokinetic profiles and reduced side effects, enhancing the likelihood of successful drug development. Although the Lipinski Rule of Five is a useful tool for predicting oral bioavailability, it should be noted that it is not a foolproof indicator of a compound's potential as a medicine. A thorough screening of all the candidates for their ADMET properties and the subsequent validation of the drug- likeness using Lipinski's rule revealed that 99% of ligands are potentially good candidates as oral drugs. Except for **L15**, all ligands exhibit high skin permeability, and 85.5% of ligands had high gastrointestinal absorption (**Table 3**).

Table 3. ADMET properties of the best 5 docked candidates.

Ligand ID	GI*1 absorption	BBB*2 permeant	LR*3	CNS*4 permeability	P-glycoprotein substrate /P-glycoprotein I inhibitor / P-glycoprotein IIinhibitor*5	CYP2D6 Substrate /CYP3A4 Substrate / CYP1A2 inhibitor /CYP2C19 Inhibitor / CYP2C9 inhibitor / CYP2D6 inhibitor / CYP3A4 inhibitor*6	hERG I inhibitor / hERG II inhibitor*7	Hepatotoxicity	Skin Sensitisition
L10	Low	No	Yes	-0.912	P-glycoprotein substrate-NO (P-glycoprotein I inhibitor/P-glycoprotein II inhibitor)-YES	CYP3A4 substrate-YES (CYP2D6 substrate/ CYP1A2 inhibitor/CYP2C19 inhibitor/ CYP2C9 inhibitor/ CYP2D6 inhibitor/ CYP3A4 inhibitor)-NO	hERG I inhibitor-No, hERG II inhibitor-Yes	NO	NO
L12	High	No	Yes	-0.885	P-glycoprotein substrate-NO (P-glycoprotein I inhibitor/P-glycoprotein II inhibitor)-YES	(CYP3A4 Substrate /CYP1A2 inhibitor)-YES (CYP2D6 substrate /CYP2C19 inhibitor / CYP2C9 inhibitor / CYP2D6 inhibitor / CYP3A4 inhibitor) -NO	hERG I inhibitor-No, hERG II inhibitor-Yes	NO	NO
L13	High	Yes	Yes	-1.771	All Yes	CYP (2D6 S // 2C19 I / 2C9 I)-NO CYP (2D6 I / 3A4I)-YES	hERG I inhibitor-No, hERG II inhibitor-Yes	YES	YES
L41	Low	NO	Yes	-1.501	All Yes	(CYP2D6 Substrate /CYP2D6 inhibitor)-NO (CYP3A4 substrate / CYP1A2 inhibitor /CYP2C19 inhibitor / CYP2C9 inhibitor / CYP3A4 inhibitor)-YES	hERG I inhibitor-No, hERG II inhibitor-Yes	NO	NO
L179	High	Yes	Yes	-1.261	P- glycoprotein (IS,)- No	CYP (2D6 S / 2D6 I/3A4 I)- NO	hERG I inhibitor-No, hERG	NO	NO
					P- glycoprotein (I In, II In)- Yes	CYP (3A4 S / 1A2I / 2C19 I / 2C9 I)- YES	II inhibitor-Yes		

*1Gastro Intestinal, *2Blood Brain Barrier, *3Lipinski's Rule of 5, *4central nervous system permeability, *5P-glycoprotein substrate, P-glycoprotein I and II inhibitor, *6CytochromeP450 substrate and inhibitors.

1.1. MD Simulation studies

The ligand **L10** showed the highest binding affinity among the ligands, hence, in addition with the apo-protein, the **L10**- protein complex was subjected to 100 ns all atoms MD simulation. The apo-protein and the protein in complex with the ligand L10 had average RMSD values of 0.252 and 0.243, respectively. In comparison to the apo-protein, the protein attached to the ligand L10 has a lower RMSD, indicating a more stable conformation. This suggests that the protein and ligand have an advantageous and persistent association throughout the simulation. (**Figure 8A**). The acceptability of the ligand as a potential drug candidate was further confirmed by assessing the robustness of the protein-ligand conjunction that is generated (**Figure 8C**), which was determined by the convergence of Root Mean Square Deviation (RMSD) plots with reasonably lower average RMSD values (**Table 4**). Significant fluctuations in RMSD could indicate potential instability within the protein-ligand complex and/or the initiation of substantial conformational alterations in the protein structure. The strong stability of the ligand **L10** inside the binding pocket was revealed by the reasonably low and stable time evolution of ligand-heavy atoms RMSD (**Figure 8B**). The C-terminus (residues 526-537) and loop regions (residues 324-342 and 410-427) displayed notably high RMSF values, with peaks exceeding 4.4 Å. Conversely, the active site of the protein (residues 346-353 and 383-404) exhibited low RMSF values, generally below 1 Å. This lower fluctuation indicates a stable core structure, likely essential for maintaining the protein's overall integrity and function. The apo-protein exhibits notable local fluctuations (avg. RMSF = 0.172 nm), while the protein-ligand complex (**L10**) shows lesser fluctuations (avg. RMSF = 0.1473 nm).

This reduction suggests that the binding of ligand **L10** contributes to a stabilizing effect on the protein, impacting its flexibility (**Figure 8D**). These RMSF findings enhance our understanding of the dynamic behavior of the protein bound to the ligand **L10** and underscore the potential stabilizing influence of the ligand on specific regions of the protein structure. practically unchanged radius of gyration and the decrease in SASA suggest that the binding of ligand **L10** results in a more compact arrangement of the protein surface (**Figures 8E and 8F**). The surface exposure change emphasizes the possible impact of ligand binding on the overall structural dynamics of the protein. (**Table 4**).

Table 4. Comparison of the geometrical parameters between the apo-protein and the complex.

Geometric parameters / System	Protein Cα RMSD (nm)	Ligand (heavy atoms) RMSD (nm)	Complex RMSD (nm)	Protein RMSF (nm)	Protein Rg (nm)	Protein SASA (nm^2)
Apo-Protein	0.252±0.0316	-	-	0.172±0.319	1.893±0.0156	141.30±4.133
Protein-Ligand (**L10**)	0.243±0.0247	0.210±0.0295	0.301±0.024	0.1473±0.122	1.896±0.0123	137.727±3.461

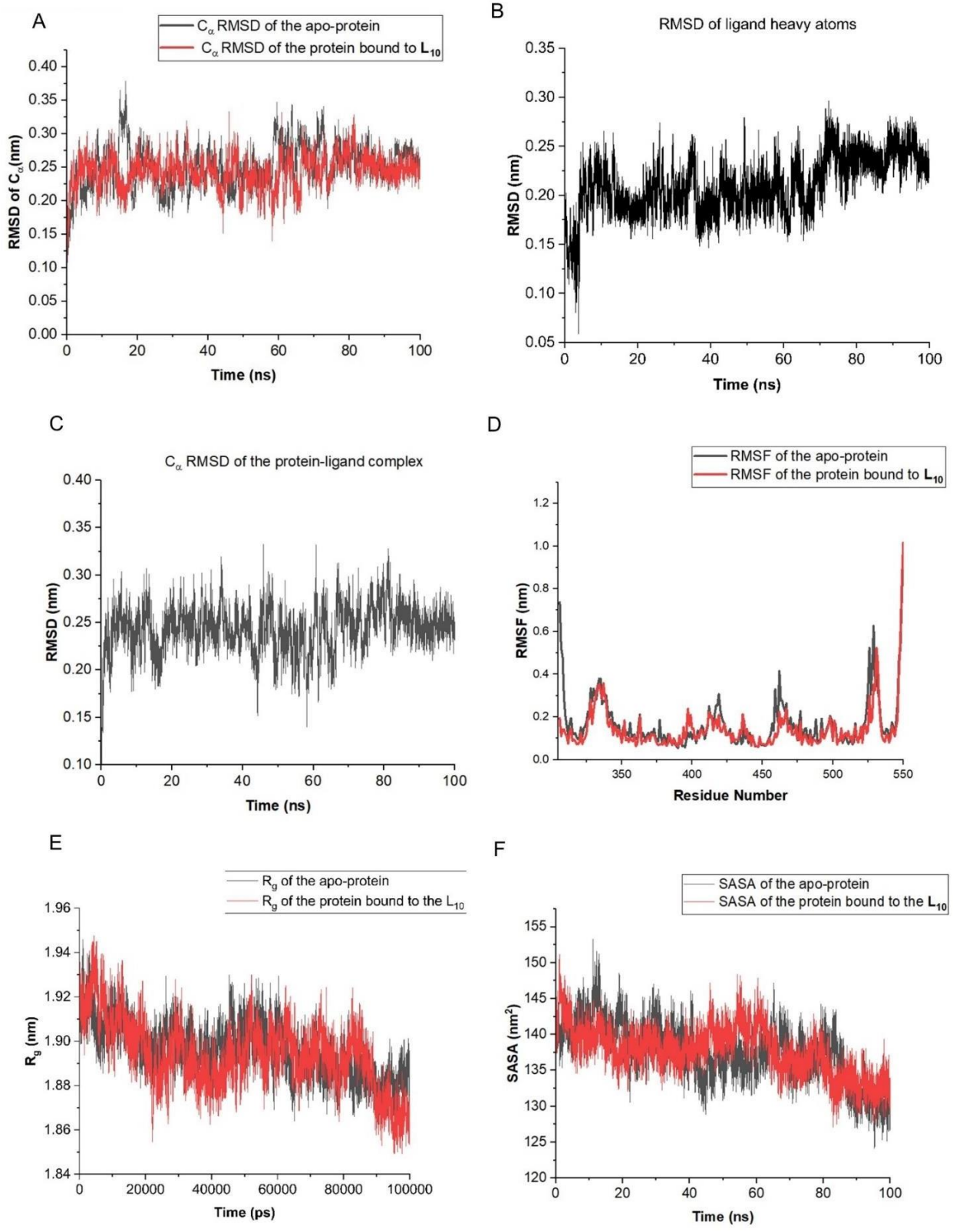

Figure 8 A) Cα RMSD (Root Mean Square Deviation) of the Protein, B) RMSD (Root Mean Square Deviation) of Ligand heavy atoms, C) Cα RMSD (Root Mean Square Deviation) of Protein-Ligand Complex, D) RMSF (Root Mean Square Fluctuations) of the protein, E) Rg (Radius

1.1. DFT studies

The optimized geometry (**Figure 9**) of the best-docked ligand (**L10**), obtained using the DFT method, was used to generate the electrostatic potential map and MO diagrams.

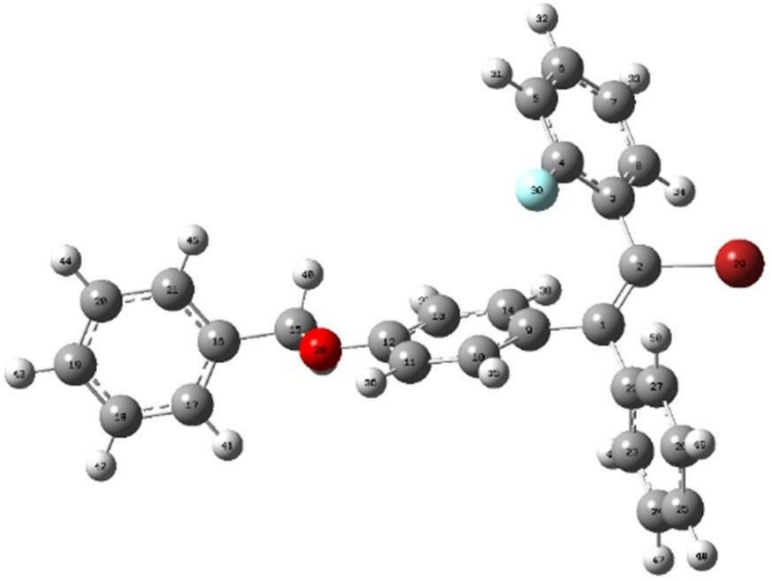

Figure 9 The Optimized Structure.

Molecular electrostatic potential surface

The distribution of charges throughout the molecule's three-dimensional surface is demonstrated by the MEP analysis. The electron-rich and electron-deficient surface areas can be distinguished from one another with the help of color grading. Based on MEP investigations, certain physicochemical characteristics of a molecule can be assessed (Murry et al, 1996 Boukabcha et al, 2015; Demir 2019). (Figure 10) shows the MEP surface for L10, with colour variations caused by charge density changes. MEP Surface visualization includes visual representations of the MEP surface, often using color coding (Typically, those with a greater number of electrons appear red, whereas those with fewer electrons appear blue). The MEP analysis revealed that the most negative potential on the molecular surface was observed at -3.704e-2 atomic units (a.u.) The strongest blue color indicated the maximum positive potential, which showed up at 3.704e-2 a.u. The strongest negative potential was reflected by the reddest hue. The region with the deepest red colour, which indicates a negative potential, was shown to be most vulnerable to electrophilic attack based on the MEP analysis. Conversely, the area with the strongest blue hue (which denotes positive potential) was found to be vulnerable to nucleophilic attack. (Campanario et al, 1994) Reddish-yellow coloration that indicates negative potential is commonly associated with atoms that have localized lone pairs of electrons, which are distinguished by electronegative centers. In **Figure 10**, the negative electrostatic potential (depicted in red) was observed over the oxygen atom (O28), bromine (Br29), and fluorine (F30). Additionally, the cyan color depicted a slightly positive electrostatic potential.

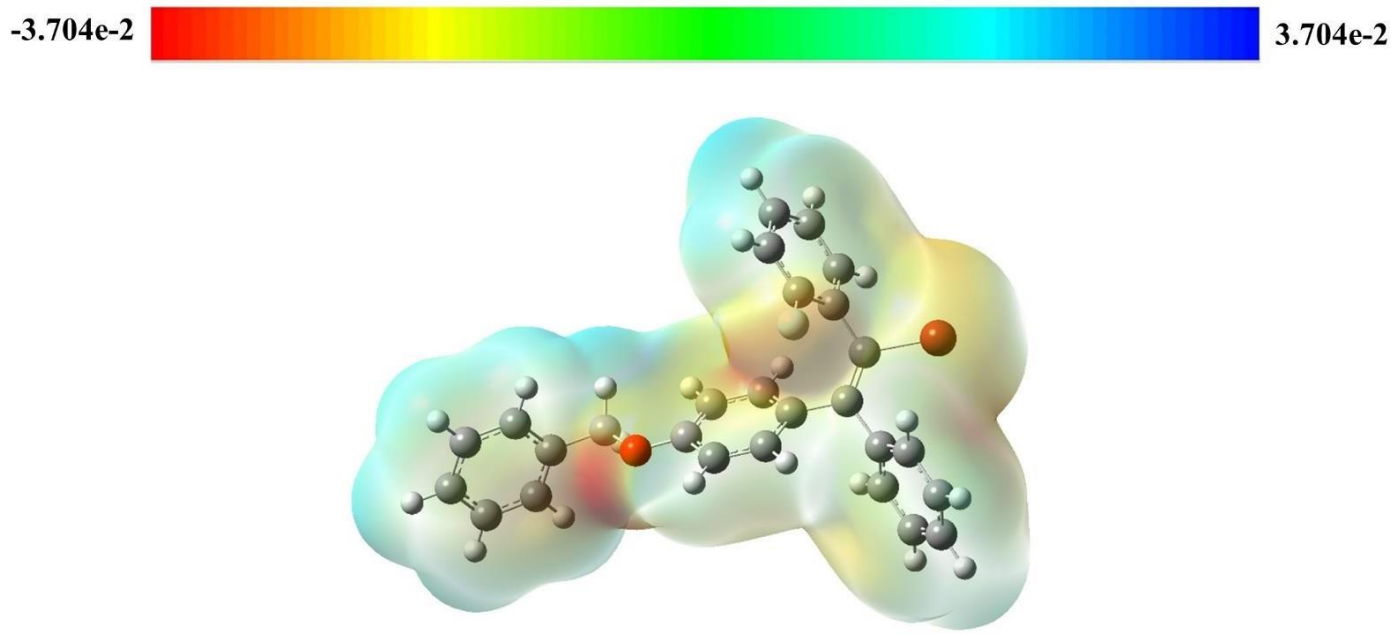

Figure 10 The surface of molecular electrostatic potential (MEP) for ligand L10.

The HOMO-LUMO energy bandgap, is a helpful metric for evaluating the stability, chemical activity, and other characteristics of a compound. Based on the energy levels of the HOMO and LUMO, the chemical hardness, electronegativity electronic chemical potential, and electrophilicity index of the molecule under study were computed. There is a 4.236 eV energy difference in both HOMO and LUMO. (**Figure 11)**, Moreover, this is a crucial factor in determining electron conductivity. Chemical hardness is a representation of the reactivity and stability of a chemical system. This descriptor is employed to quantify the molecule's capacity to resist alterations in electron distribution or charge (**Table 5)**. The molecule's chemical hardness was found to be 2.118, which is a rather large value that suggests chemical consistency. Additionally, it was found that the electronegativity value, which quantifies a molecular species and represents an atom's capacity to attract electrons within a molecule, was 3.732 (Parthasarathi et al, 2004). It was calculated that the ability to attract electrons amounted 3.287.

Table 5. Calculated values of some important electronic parameters for **L10**

Parameters	Values
E_{HOMO} (eV)	-5.851
E_{LUMO} (eV)	-1.614
Ionization potential (eV)	5.851
Electron affinity (eV)	1.614
Energy gap (eV)	4.236

Parameters	Values
Electronegativity (eV)	3.732
Chemical potential (eV)	-3.732
Chemical hardness (eV)	2.118
Chemical softness (eV)	0.236
Electrophilicity index (eV)	3.287

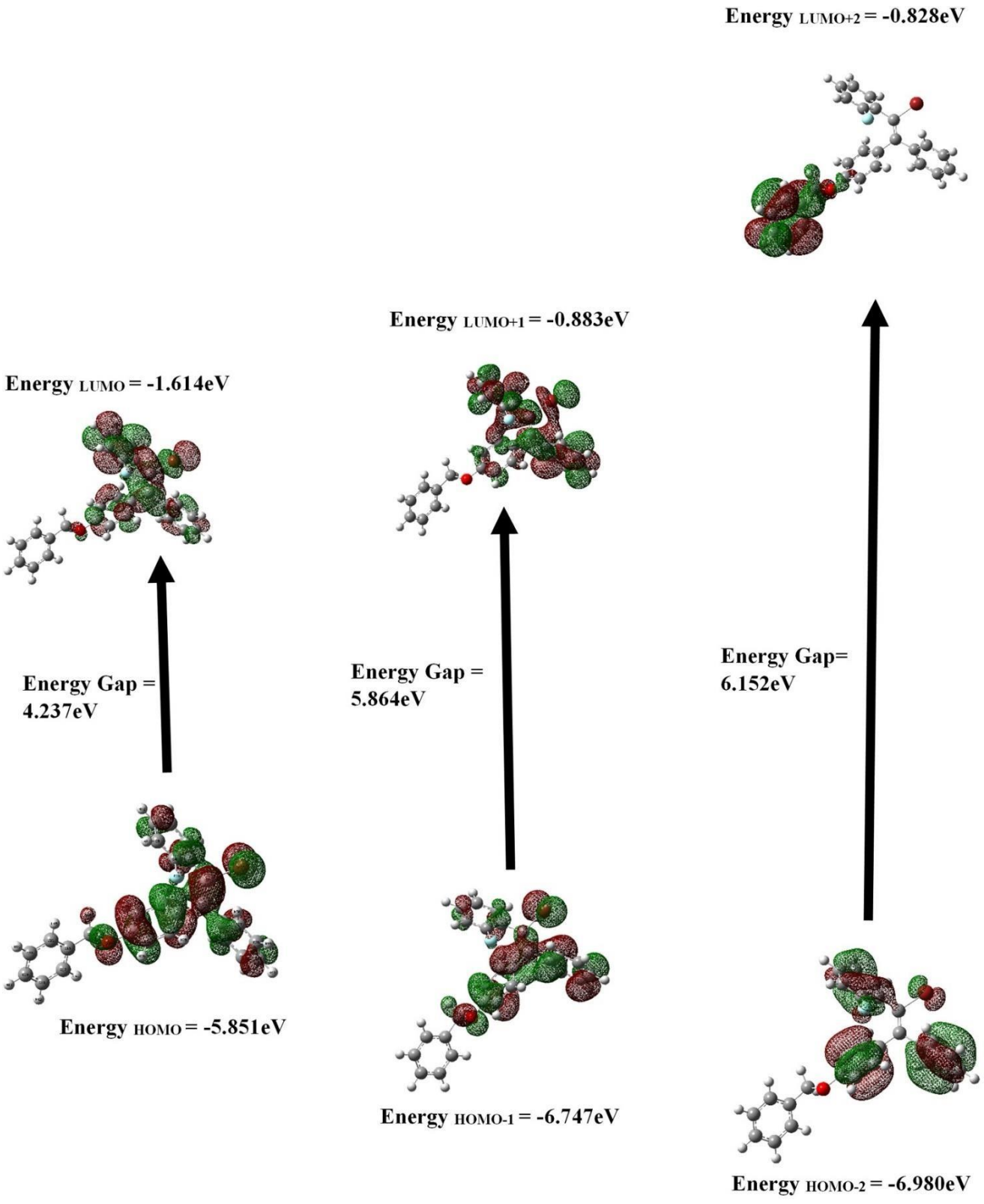

Figure 11 Key molecular orbitals (MOs) of L10 and their respective energy values.

2. Conclusion

L10 emerged to be a strong potential candidate for becoming an inhibitor for ERα with high binding affinity (-12.311 kcal/mol) along with reasonably stable time evolution of the protein Cα, practically unchanged radius of gyration, low RMSF value for the active site residues, and low SASA as compared to the apo-protein. Further, the drug-likeness of the concerned ligand was found to be high as interpreted from the ADMET studies. The DFT studies revealed its HOMO-LUMO gap to be 4.237eV. This potential hit candidate (**L10**) remains to be subjected to *in vitro* and subsequent *in vivo* studies for further validation. In the future, we wish to screen a bigger chemical space generated using active-site-directed pharmacophore mapping, against the given receptor to identify potentialleads.

3. Acknowledgement

The authors thank Mrinalini Datta Mahavidyapith for the infrastructural support.

4. Author's Contribution

Conceptualization – P.B. Designing Computational Studies – P.B. Performing Computational Studies – Z.W., and P.B. Manuscript Writing – Z.W., and P.B. with support from P.D. and S.K.

5. Conflict of Interest

There is no conflict of interest, according to the authors.

Graphical Abstract

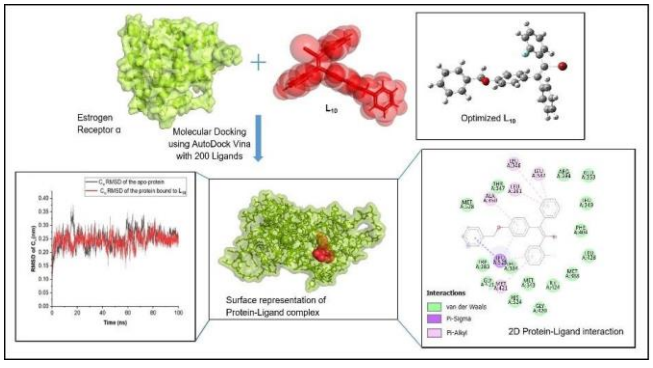

REFERENCES

1. https://www.webmd.com/breast-cancer/breast-cancer-types-er-positive-her2-positive
2. Chen, Y., Li, H., Janowczyk, A., Toro, P., Corredor, G., Whitney, J., Lu, C., Koyuncu, C. F., Mokhtari, M., Buzzy, C., Ganesan, S., Feldman, M. D., Fu, P., Corbin, H., Harbhajanka, A., Gilmore, H., Goldstein, L. J., Davidson, N. E., Desai, S. & Madabhushi, A. (**2023**) Computational pathology improves risk stratification of a multi-gene assay for early-stage ER+ breast cancer. *Npj Breast Cancer, 9*, 1-10. https://doi.org/10.1038/s41523-023-00545-y
3. Chen, S. (**2011**). An "Omics" Approach to Determine the Mechanisms of Acquired Aromatase Inhibitor Resistance. *OMICS: A Journal of Integrative Biology*, *15*, 347-352. https://doi.org/10.1089/omi.2010.0097
4. Davies, K. J. A., Godwin, J., Gray, R., Clarke, M., Cutter, D. J., Darby, S. C., McGale, P., Pan, H., Taylor, C., Wang, X., Dowsett, M., Ingle, J. N. & Pető, R. (**2011**). Relevance of Breast Cancer Hormone Receptors and Other Factors to the Efficacy of Adjuvant Tamoxifen: Patient-Level Meta-Analysis of Randomised Trials. *The Lancet*, *378* (9793), 771–784. https://doi.org/10.1016/s0140-6736(11)60993-8.
5. Nicholson, R. I. & Johnston, S. (**2005**). Endocrine Therapy – Current Benefits and Limitations. *Breast Cancer Research and Treatment*, *93* (S1), 3–10. https://doi.org/10.1007/s10549-005-9036-4.
6. Osborne, C. K. & Schiff, R. (2011). Mechanisms of Endocrine Resistance in Breast Cancer. *Annual Review of Medicine*, *62* (1), 233–247. https://doi.org/10.1146/annurev-med-070909-182917.
7. Hanker, A. B., Sudhan, D. R. & Arteaga, C. L. (2020). Overcoming Endocrine Resistance in Breast Cancer. *Cancer Cell*, *37* (4), 496–513. https://doi.org/10.1016/j.ccell.2020.03.009.
8. Research, C. for D. E. A. *FDA approves elacestrant for ER-positive, HER2-negative, ESR1-mutated advanced or metastatic breast cancer*. U.S. Food And Drug Administration. https://www.fda.gov/drugs/resources-information-approved-drugs/fda-approves-elacestrant-er-positive-her2-negative-esr1-mutated-advanced-or-metastatic-breast-cancer.
9. Hsu, J. L. & Hung, C. (2016). The role of HER2, EGFR, and other receptor tyrosine kinases in breast cancer. *Cancer metastasis reviews*, *35*(4), 575. https://doi.org/10.1007/s10555-016-9649-6
10. Miricescu, D., Totan, A., Badoiu, S. C., Stefani, C. & Greabu, M. (**2021**). PI3K/AKT/mTOR Signaling Pathway in Breast Cancer: From Molecular Landscape to Clinical Aspects. *International Journal of Molecular Sciences*, *22*(1), 173. https://doi.org/10.3390/ijms22010173
11. Edris, A., Abdelrahman, M., Osman, W., Sherif, A. E., Ashour, A., Garelnabi, E. A., Ibrahim, S. R., Bafail, R., Samman, W. A., Ghazawi, K. F., Mohamed, G. A. & Alzain, A. A. (2023). Design of Novel Letrozole Analogues Targeting Aromatase for Breast Cancer: Molecular Docking, Molecular Dynamics, and Theoretical Studies on Gold Nanoparticles. Metabolites, *13*, 583. https://doi.org/10.3390/metabo13050583
12. Lee, J. S., Hackbart, H., Cui, X. & Yuan, Y. (**2023**). CDK4/6 Inhibitor Resistance in Hormone Receptor-Positive Metastatic Breast Cancer: Translational Research, Clinical Trials, and Future Directions. *International Journal of Molecular Sciences*, *24*(14), 11791. https://doi.org/10.3390/ijms241411791
13. https://www.cancer.gov/about-cancer/causes-prevention/genetics/brca-fact-sheet

14. Yager, J. D. & Davidson, N. E. (**2006**). Estrogen Carcinogenesis in Breast Cancer. *The New England Journal of Medicine 354* (3), 270–282. https://doi.org/10.1056/nejmra050776.
15. Rocha-Roa, C., Cortes, E., Cuesta, S., Mora, J. R., De Paz, J. L. C., Flores-Sumoza, M. & Márquez, E. (**2023**). Study of Potential Inhibition of the Estrogen Receptor α by Cannabinoids Using an in Silico Approach: Agonist vs Antagonist Mechanism. *Computers in Biology and Medicine 152*, 106403. https://doi.org/10.1016/j.compbiomed.2022.106403.
16. Pettersen, E. F., Goddard, T. D., Huang, C. C., Couch, G. S., Greenblatt, D. M., Meng, E. C. & Ferrin, T. E. (**2004**). UCSF Chimera−a visualization system for exploratory research and analysis. *J. Comput. Chem. 25*, 1605−1612
17. Gasteiger, J. & Marsili, M. (1978). A new model for calculating atomic charges in molecules. *Tetrahedron Lett. 19*, 3181−3184
18. Morris, G. M., Huey, R., Lindstrom, W., Sanner, M. F., Belew, R. K., Goodsell, D. S. & Olson, A. J. (**2009**). Autodock4 and AutoDockTools4: automated docking with selective receptor flexiblity. J. *Computational Chemistry***.** *16*: 2785-91.
19. Saha, T., Makar, S., Swetha, R., Gutti, G. & Singh, S. K. (**2019**). Estrogen Signaling: An Emanating Therapeutic Target for Breast Cancer Treatment. *European Journal of Medicinal Chemistry 177*, 116–143. https://doi.org/10.1016/j.ejmech.2019.05.023.
20. Eberhardt, J., Santos-Martins, D., Tillack, A. F. & Forli, S. (**2021**). AutoDock Vina 1.2.0: New Docking Methods, Expanded Force Field, and Python Bindings. *J. Chem. Inf. Model. 61*, 3891−3898.
21. Trott, O. & Olson, A. J. (**2009).** AutoDock Vina: Improving the speed and accuracy of docking with a new scoring function, efficient optimization, and multithreading. *J. Comput. Chem. 31*, 455−461.
22. Daina, A., Michielin, O., & Zoete, V. (**2017**). SwissADME: A free web tool to evaluate pharmacokinetics, drug-likeness, and medicinal chemistry friendliness of small molecules. *Scientific Reports*. *7*, 1-13. https://doi.org/10.1038/srep42717.
23. Pires, D. E. V., Blundell, T. L. & Ascher, D. B. (**2015**). pkCSM: Predicting Small-Molecule Pharmacokinetic and Toxicity Properties Using Graph-Based Signatures. Journal of Medicinal Chemistry, *58*, 4066–4072. doi: 10.1021/acs.jmedchem.5b00104
24. Lipinski C. A., Lombardo F., Dominy B.W., Feeney P.J. (2001). Experimental and computational approaches to estimate solubility and permeability in drug discovery and development settings. *Adv Drug Deliv Rev. 46*, 3-26
25. Bauer, P., Hess, B. & Lindahl, E. (**2022).** GROMACS
42. *12* 5533-5543.
Source code
26. Huang, J., MacKerell, A.D., Comput. J. Chem. *34* **2013** 2135
27. Zoete, V., Cuendet, M. A., Grosdidier, A. & Michielin, O. (**2011).** SwissParam: A fast force field generation tool for small organic molecules. *J. Comput. Chemistry, 32* 2359–2368.
28. Mark, P. & Nilsson, L. (2001). Structure and Dynamics of the TIP3P, SPC, and SPC/E Water Models at 298 K. J. Phys. Chem. A *105*, 9954–9960.
29. Boonstra, S., Onck, P. R. & van der Giessen E. (2016). *J. Phys. Chem.* B *120* 3692–3698
30. Frisch, M. J., Trucks, G. W., Schlegel, H. B., Scuseria, G. E., Robb, M. A., Cheeseman, J. R., Scalmani, G., … (2016). Gaussian 09, Revision A.02, Gaussian, Inc; Wallingford CT, 2016.
31. Petersson, G. A., Bennet, A., Tensfeldt, T.G., Al-Laham, M.A., Shirley, W.A. & Mantzaris, (1988). J. J. Chem. Phys. *89* (4) 2193-2218.
32. Koopmans, T. (1934). *Physica 1* 104-113.
33. J.S. Murry, K. Sen, (1996). Molecular Electrostatic Potential Concepts and Applications, Elsevier, Amesterdam,.
34. Boukabcha, N., Djafri, A., Megrouss, Y., Tamer, Ö., Avcı, D., Tuna, M., Dege, N., … (2015). *Mol. Struct.* 1100 112-123.
35. Demir, S., Cakmak, S., Dege, N., Kutuk, H., Odabasoglu, M. & Kepekci, R. A. (2019). *J. Mol. Struct. 1194* 582-591.
36. Debnath, P., Bhaumik, S., Sen, D., Muttineni, R. K. & Debnath, S. (**2021**). Identification of SARS-COV-2 Main Protease Inhibitors Using Structure Based Virtual Screening and Molecular Dynamics Simulation of DrugBank Database. *Chemistry Select 6* (20), 4991–5013. https://doi.org/10.1002/slct.202100854.
37. Kumar, R., Zakharov, M. N., Khan, S. H., Miki, R., Jang, H., Toraldo, G., Singh, R., Bhasin, S. & Jasuja, R. (**2011)**. The Dynamic Structure of the Estrogen Receptor. *Journal of Amino Acids*, https://doi.org/10.4061/2011/812540
38. Shiau, A. K., Barstad, D., Loria, P. M., Cheng, L., Kushner, P. J., Agard, D. A. & Greene, G. L. (**1998**). The Structural Basis of Estrogen Receptor/Coactivator Recognition and the Antagonism of This Interaction by Tamoxifen. *Cell 95* (7), 927–937. https://doi.org/10.1016/s0092-8674(00)81717-1.
39. Campanario, J. M. Bronchalo, E. Hidalgo, M. A. *J. Chem. Educ. 71* 1994 761-766.
40. Lakshminarayanan, S., Jeyasingh, V., Murugesan, K. & Selvapalam, Dass, N. G. (2021) *J. Photochem. Photobiol.* 6 100022.
41. Parthasarathi, R., Subramanian, V., Roy, D.R. & Chattaraj, P.K. Bioorg. (2004). *Med. Chem.*